ELSEVIER

Chemical Engineering Journal 87 (2002) 41–48

Chemical Engineering Journal

www.elsevier.com/locate/cej

Dilute gas–solid flow in a riser

G. Ferschneider*, P. Mège

Institut Français du Pétrole, BP 3, 69390 Vernaison, France

Received 9 October 2000; received in revised form 9 October 2000; accepted 5 July 2001

Abstract

The hydrodynamic behaviour of dispersed gas–solid flow in a riser is simulated using the two-fluid model formalism, with complementary information from the kinetic theory of granular media to represent the transport properties of the solid phase. The specific source terms of phases interaction are described in the momentum transport and fluctuating kinetic energy equations of each phase. The simulation results show the highly unsteady state of the flow. Inspection of the kinematic parameters fluctuations confirms these results. The core–annulus structure and the existence of clusters are well predicted.

Keywords: Gas–solid flow; Riser; Core–annulus structure

1. Introduction

Dilute gas–solid flows are used in ultra-rapid gas-phase catalytic reactions with the solid particles as catalysts. Their principal advantages are that they ensure optimal conditions: high temperatures and short contact times. Major applications are fluid catalytic cracker (FCC) risers and circulating fluidized bed (CFB) combustors. However, the transfer mechanisms within the dilute gas–solid flow are still not well understood. A dilute gas–solid flow is made up of coexisting very dilute (core) and dense (cluster, annulus) regions. Therefore, the hydrodynamic model must take into account simultaneously the gas–particle and particle–particle interactions in the mean and fluctuating motion by entrainment and interparticle collision mechanisms.

The approach used is that developed by Simonin and coworkers [1–3] based on the two-fluid model. The transport properties of the solid phase are obtained by applying the kinetic theory of gases while taking into account the influence of the interstitial gas.

2. Transport equations: average fields

The transport equations describing gas–solid turbulent two-phase flow may be derived by applying the conditional phase-averaging method for the gas and the kinetic theory formalism for the discrete particle. In the following, subscript k refers to each phase ($k = 1$ for the gas and $k = 2$ for the particles).

- *Mass balance*:

$$\frac{\partial}{\partial t}\alpha_k\rho_k + \frac{\partial}{\partial x_i}\alpha_k\rho_k U_{k,i} = 0 \tag{1}$$

where α_k is the mean volumetric fraction and ρ_k the density of the phase k. $U_{k,i} = \langle u_{k,i}\rangle_k$ represents the mean velocity component of the phase k defined by the conditional volumetric phase average $\langle\,\rangle_k$. It complies with the fluctuating velocity $u''_{k,i} = u_{k,i} - U_{k,i}$.

- *Momentum balance*:

$$\frac{\partial}{\partial t}\alpha_k\rho_k U_{k,i} + \frac{\partial}{\partial x_j}\alpha_k\rho_k U_{k,j}U_{k,i} = -\alpha_k\frac{\partial P_1}{\partial x_i} - \frac{\partial}{\partial x_j}\Sigma_{k,ij} + \alpha_k\rho_k g_i + I_{k,i} \tag{2}$$

where P_1 is the mean pressure of the gas, $\Sigma_{k,ij}$ represents the effective stress tensor in the k phase, and $I_{k,i}$ corresponds to the inter-phase momentum exchange after subtracting the contribution due to the mean gas-pressure gradient.

- *Momentum transfer*: The interfacial momentum exchange is modelled in the specific case of gas–solid flow implying large and heavy particle $\rho_2/\rho_1 \gg 1$. In this case, the forces due to the gas on a single particle reduce to the mean pressure gradient and to the drag. The corresponding term in the mean momentum equation can be written as

$$I_{2,i} = -I_{1,i} = -\frac{\alpha_2\rho_2 V_{\mathrm{r},i}}{\tau_{12}^{\mathrm{F}}}$$

* Corresponding author. Fax: +33-4-78-02-20-09.
E-mail address: gilles.ferschneider@ifp.fr (G. Ferschneider).

1385-8947/02/$ – see front matter
PII: S1385-8947(01)00207-8

Nomenclature

C_D	drag coefficient (–)
d	particle diameter (m)
e_c	coefficient of elastic restitution (–)
g	gravity (m s^{-2})
g_0	pair-correlation function (–)
I	inter-phase momentum exchange (kg m^{-2} s^{-2})
K	diffusion coefficient (m^2 s^{-1})
P	pressure (Pa)
q_{12}	gas–particle velocity correlation (m^2 s^{-2})
q^2	turbulent kinetic energy (m^2 s^{-2})
R	kinetic stress tensor (m^2 s^{-2})
Re	Reynolds number (–)
S	velocity third-order moment tensor (m^3 s^{-3})
t	time (s)
$u''_{k,i}$	ith component of fluctuating velocity vector for phase k (m s^{-1})
$U_{k,i}$	ith component of mean velocity vector for phase k (m s^{-1})
$V_{d,i}$	ith component of drift velocity vector (m s^{-1})
$V_{r,i}$	ith component of relative velocity vector (m s^{-1})
x	spatial coordinate (m)

Greek symbols

α	volumetric fraction (–)
ϵ	turbulent dissipation (m^2 s^{-3})
$\Theta_{k,ij}$	shear tensor for phase k (kg m^{-1} s^{-2})
λ	granular viscosity (Pa s)
μ	dynamic viscosity (Pa s)
ν	kinematic viscosity (m^2 s^{-1})
ξ	collisional constant (–)
Π	source term of turbulent kinetic energy (kg m s^{-3}, kg m s^{-4})
ρ	density (kg m^{-3})
σ	collisional constant (–)
$\Sigma_{k,ij}$	effective stress tensor for phase k (kg m^{-1} s^{-2})
τ	characteristic time (s)
ϕ	correction function due to inelasticity of collision (–)
χ_{ij}	vector of collisional source term for fluctuating particle energy (kg m^{-1} s^{-3})

Index

c	collisional
f	fluidization
fp	primary fluidization
fs	secondary fluidization
g	gas
i, j, m	spatial coordinates
k	phase; $k = 1$: gas, $k = 2$: solid, $k = 12$: gas–solid covariance
mf	minimum of fluidization
s	solid
t	turbulent
tv	terminal velocity

Subscripts

c	collisional
f	fluid
F	entrainment by fluid
kin	kinetic
t	turbulent

Operators

$\langle\cdot\rangle$	volumetric phase average
$\partial/\partial x_i$	gradient
$\partial/\partial x_j$	transposed gradient
$\partial/\partial x_m$	divergence
$\lvert\cdot\rvert$	norme
δ_{ij}	Kronecker operator

where τ_{12}^F is the characteristic time-scale of gas–particle momentum transfer, or particle relaxation time. The mean relative velocity $V_{r,i} = [U_{2,i} - U_{1,i}] - V_{d,i}$ in which the drifting velocity $V_{d,i}$ represents the difference due to the correlation between the instantaneous distribution of the particle and the fluid turbulent velocity. This term is modelled as a diffusion term [8]. The dispersion coefficient is a function of a characteristic time of turbulence related to the particle and the two-phase fluctuating velocity covariance:

$$V_{d,i} = -D^t_{12,ij}\frac{1}{\alpha_1\alpha_2}\frac{\partial\alpha_2}{\partial x_j}, \qquad D^t_{12,ij} = \tau^t_{12}\langle u''_{1,i}u''_{2,j}\rangle_2$$

The time-scale τ_{12}^F is based on an empirical relationship. For dilute gas–solid flow, the starting point is the Stokes law modified in order to account for Reynolds number influence and the concentration effects [4]. In dense gas flow, a correlation based on Ergun's relation [5] is used:

- $\alpha_2 < 0.2$:

$$\frac{1}{\tau_{12}^F} = \frac{3}{4}\frac{\rho_1}{\rho_2}\frac{C_D}{d}\alpha_1^{-1.7}\langle|V_r|\rangle, \qquad Re = \frac{\alpha_1\langle|V_{r,i}|\rangle d}{\nu_1},$$

$$C_D = \begin{cases} \dfrac{24}{Re}[1 + 0.15\,Re^{0.687}], & Re < 1000 \\ 0.44, & Re \geq 1000 \end{cases}$$

- $\alpha_2 \geq 0.2$:

$$\frac{1}{\tau_{12}^F} = \frac{\rho_1}{\rho_2}\left[\alpha_2\frac{150}{Re} + 1.75\right]\frac{1}{d}\langle|V_r|\rangle$$

3. Transport equations: fluctuating fields

3.1. Fluctuating particle motion

A statistical approach is used to determine the transport properties of the solid phase. The particle–particle collisions are taken into account and considered to be inelastic with a coefficient of restitution e_c ($0 < e_c < 1$). The development of this approach leads to an expression of the solid-phase effective stress tensor in two parts [6,7]:

$$\Sigma_{2,ij} = \alpha_2 \rho_2 R_{2,ij} + \Theta_{2,ij}$$

The first part $R_{2,ij} = \langle u''_{2,i} u''_{2,j} \rangle_2$ represents the kinetic contribution which corresponds to the second-order tensor of the velocity fluctuations representing the transport of momentum by the particles between collisions.

The second part, $\Theta_{2,ij}$, represents the momentum transport due to particle–particle collisions. The transport equations for each component of the kinetic portion of the tensor have been developed by He and Simonin [8] and are written in the following form:

$$\begin{aligned}
&\alpha_2\rho_2\left(\frac{\partial R_{2,ij}}{\partial t} + U_{2,k}\frac{\partial R_{2,ij}}{\partial x_k}\right) \\
&\quad = -\frac{\partial}{\partial x_k}(\alpha_2\rho_2 S_{2,ijk} + \Theta_{2,ijk}) - \frac{\alpha_2\rho_2}{\tau_{12}^{\mathrm{F}}}(R_{2,ij} \\
&\qquad - R_{12,ij}) - (\alpha_2\rho_2 R_{2,ik} + \Theta_{2,ik})\frac{\partial U_{2,j}}{\partial x_k} \\
&\qquad - (\alpha_2\rho_2 R_{2,jk} + \Theta_{2,jk})\frac{\partial U_{2,i}}{\partial x_k} + \chi_{ij}
\end{aligned} \tag{3}$$

The first term on the right-hand side of this equation is interpreted as a diffusion term and represents the transport of kinetic stress by the fluctuating motion $S_{2,ijk} = \langle u''_{2,i} u''_{2,j} u''_{2,k} \rangle$ and the collisions. The second term represents the interactions between the fluctuating motion of the particles and the gas, which leads to a local destruction or production of kinetic stress, depending on the value of the fluid–particle correlation tensor:

$$R_{12,ij} = \tfrac{1}{2}(\langle u''_{1,i} u''_{2,j} \rangle_2 + \langle u''_{2,i} u''_{1,j} \rangle_2)$$

The third and fourth terms represent the creation of kinetic stress by the mean solid velocity gradients. The last term, relative to the collisions, contributes to the isotropic nature of the stress tensor and to its destruction in the case of inelastic collisions.

In practice, the effects of transport and diffusion on the kinetic stresses were negligible. An equilibrium between the production and dissipation terms may be reached when the gradient of the solid mean velocity remains small compared to the inverse dissipative time-scale. This time-scale takes the form of a competition between particle relaxation time and the interparticle collision time: $(1/\tau_2^{\mathrm{t}}) = (2/\tau_{12}^{\mathrm{F}}) + (\sigma_c/\tau_2^{\mathrm{c}})$. Under these assumptions and assuming isotropic kinetic stresses, this leads to a practical form of the effective solid stress tensor, including collisional effects:

$$\begin{aligned}
\Sigma_{2,ij} &= \left[P_2 - \lambda_2\frac{\partial U_{2,m}}{\partial x_m}\right]\delta_{ij} \\
&\quad -\mu_2\left[\frac{\partial U_{2,i}}{\partial x_j} + \frac{\partial U_{2,j}}{\partial x_i} - \frac{2}{3}\frac{\partial U_{2,m}}{\partial x_m}\delta_{ij}\right]
\end{aligned} \tag{4}$$

where $P_2 = \frac{2}{3}(\alpha_2\rho_2 q_2^2[1 + 2\alpha_2 g_0(1 + e_c)])$ is the granular pressure, $\lambda_2 = \frac{4}{3}(\alpha_2^2\rho_2 d g_0(1+e_c)[(2/3)(q_2^2/\pi)]^{1/2})$ the granular viscosity, and $\mu_2 = \alpha_2\rho_2[\nu_2^{\mathrm{kin}} + \nu_2^{\mathrm{c}}]$ the shear viscosity.

The expressions for the kinetic and collisional parts of the shear viscosity are obtained from the extra-diagonal correlation transport equations for a homogeneous shear flow:

$$\begin{aligned}
\nu_2^{\mathrm{kin}} &= \left[\frac{1}{3}\tau_{12}^{\mathrm{t}} q_{12} + \frac{1}{2}\tau_{12}^{\mathrm{F}}\frac{2}{3}q_2^2(1 + \alpha_2 g_0\phi_c)\right] \\
&\quad \times\left[1 + \frac{\sigma_c}{2}\frac{\tau_{12}^{\mathrm{F}}}{\tau_2^{\mathrm{c}}}\right]^{-1}
\end{aligned} \tag{5}$$

$$\nu_2^{\mathrm{c}} = \frac{4}{5}\alpha_2 g_0(1 + e_c)\left(\nu_2^{\mathrm{kin}} + d\sqrt{\frac{2}{3}\frac{q_2^2}{\pi}}\right) \tag{6}$$

with $\sigma_c = \frac{1}{5}(1 + e_c)(3 - e_c)$ and $\phi_c = \frac{2}{5}(1 + e_c)(3e_c - 1)$ and the characteristic time between collisions

$$\tau_2^{\mathrm{c}} = \left(\frac{6\alpha_2 g_0}{d}\sqrt{\frac{16}{\pi}\frac{2}{3}q_2^2}\right)^{-1},$$

$$g_0 = \left(1 - \frac{\alpha_2}{\alpha_{2m}}\right)^{-2.5\alpha_{2m}}, \quad \alpha_{2m} = 0.64$$

The pair-correlation function g_0 is introduced to take into account the increase in the number of collisions when the volume fraction of solids approaches the maximum value $\alpha_{2m} = 0.64$ for a random packing of spheres with the same diameter.

The resulting viscosity expression is consistent with the known limits; for very diluted suspensions, it is controlled by the fluid turbulence (Tchen's theory), and in the dense limit it is controlled by the interparticle collisions. In the intermediate regime, there is a competition between the different mechanisms according to the characteristic time-scales. It may be remarked that the solid kinetic viscosity is a function of the particle relaxation time τ_{12}^{F}, implying a mean free path controlled either by the distance between two collisions or by friction with the gas. In practical configurations such as when the solid volumetric fraction is very low (<0.5% typically), collisions between particles are infrequent. In this case, the predicted mean free path larger than the duct diameter itself requires a Knudsen-type correction.

The granular pressure and solid-phase effective viscosity are written as a function of the fluctuating kinetic energy

$q_2^2 = \frac{1}{2}\langle u''_{2,i} u''_{2,i}\rangle_2$ defined by an additional transport equation obtained by summing the diagonal part of the kinetic stress transport equations:

$$\frac{\partial \alpha_2\rho_2 q_2^2}{\partial t} + \frac{\partial \alpha_2\rho_2 U_{2,j} q_2^2}{\partial x_j} = -\Sigma_{2,ij}\frac{\partial U_{2,i}}{\partial x_j} + \frac{\partial}{\partial x_j}\left[\alpha_2\rho_2(K_2^{\mathrm{kin}} + K_2^{\mathrm{c}})\frac{\partial q_2^2}{\partial x_i}\right] - \alpha_2\rho_2\frac{1}{\tau_{12}^{\mathrm{F}}}(2q_2^2 - q_{12}) - \alpha_2\rho_2\frac{1}{3}\frac{1-e_{\mathrm{c}}^2}{\tau_2^{\mathrm{c}}}q_2^2 \quad (7)$$

The right-hand side of this equation includes the production term due to the gradient of the mean velocity, the diffusion term, and the destruction terms caused by the interactions with the fluctuating motion of the gas and the inelastic collisions. The effective diffusivity is also decomposed in the form of kinetic and collisional contributions:

$$K_2^{\mathrm{kin}} = \left[\frac{1}{3}\tau_{12}^{\mathrm{t}} q_{12} + \frac{5}{9}\tau_{12}^{\mathrm{F}}\frac{2}{3}q_2^2(1+\alpha_2 g_0\varphi_{\mathrm{c}})\right] \times \left[1 + \frac{5}{9}\xi_{\mathrm{c}}\frac{\tau_{12}^{\mathrm{F}}}{\tau_2^{\mathrm{c}}}\right]^{-1} \quad (8)$$

$$K_2^{\mathrm{c}} = \alpha_2 g_0(1+e_{\mathrm{c}})\left(\frac{6}{5}K_2^{\mathrm{kin}} + \frac{4}{3}d\sqrt{\frac{2}{3}\frac{q_2^2}{\pi}}\right) \quad (9)$$

with $\xi_{\mathrm{c}} = \frac{1}{100}(1+e_{\mathrm{c}})(49-33e_{\mathrm{c}})$ and $\varphi_{\mathrm{c}} = \frac{3}{5}(1+e_{\mathrm{c}})^2(2e_{\mathrm{c}}-1)$.

3.2. Gas turbulence

The modelling of the gas-phase effective stress tensor is performed in the framework of the classical turbulent eddy viscosity mode $q_1^2 - \epsilon$ in which particle influence is taken into account. The drag force due to particles in the gas momentum equation introduces an extra term in the fluctuating kinetic energy transport equation for the gas phase, $\Pi_{q_1} = -\alpha_2\rho_2(1/\tau_{12}^{\mathrm{F}})(2q_1^2 - q_{12} - V_{\mathrm{d}}V_{\mathrm{r}})$, and the corresponding term in the ϵ transport equation. For gas–solid flows, the term Π_{q_1} generally leads to a destruction of the turbulent kinetic energy thus decreasing the turbulent viscosity. Finally, the gas–particle velocity correlation, q_{12}, is determined from a semi-empirical transport equation [5]:

$$\frac{\partial \alpha_2\rho_2 q_{12}}{\partial t} + \frac{\partial \alpha_2\rho_2 U_{2,j} q_{12}}{\partial x_j} = \frac{\partial}{\partial x_j}\left[\alpha_2\rho_2\frac{\nu_{12}^{\mathrm{t}}}{\sigma_q}\frac{\partial q_{12}}{\partial x_i}\right] - \alpha_2\rho_2\epsilon_{12} + \Pi_{q_{12}} - \alpha_2\rho_2\langle u''_{1,i}u''_{2,j}\rangle_2\frac{\partial U_{2,i}}{\partial x_j} - \alpha_2\rho_2\langle u''_{2,i}u''_{1,j}\rangle_2\frac{\partial U_{1,i}}{\partial x_j} \quad (10)$$

with $\epsilon_{12} = q_{12}/\tau_{12}^{\mathrm{t}}$ and $\Pi_{q_{12}} = -(\alpha_2\rho_2/\tau_{12}^{\mathrm{F}})[(1+X_{21})q_{12} - 2q_1^2 - 2X_{21}q_2^2]$, $X_{12} = \alpha_2\rho_2/\alpha_2\rho_2$

The first term on the right-hand side represents the covariance transport by the fluctuating velocity. The second one takes into account the destruction by the fluid viscosity and the decorrelation of the fluctuating motion due to the slip between the phases. The third one characterizes the interaction with the fluctuating motion of each phase. The two last terms represent production due to the mean velocity gradient.

4. Basic mechanisms and flow regimes

The elementary mechanisms of gas–particle and particle–particle interactions taken into consideration are:

- Gas-phase turbulence and its Lagrangian time-scale τ_1^{t}.
- The coupling between the fluctuating motion of the gas and the agitation of the particles characterized by τ_{12}^{t}, the fluctuation time of the fluid as seen by the particles.
- The entrainment of the solid particles by the motion of the gas, with which is associated the relaxation time τ_{12}^{F}, a characteristic of the inertia of the particles.
- The collisions with τ_2^{c}, the characteristic time between the collisions.

The last two mechanisms involve the fluctuating motion of the particles characterized by the contact time τ_2^{t}.

In order to quantify the importance of the different physical mechanisms involved in gas–solid flow, their time-scales can be compared:

- $\tau_1^{\mathrm{t}} < \tau_2^{\mathrm{t}}$: the dominant mechanisms are inherent to the gas phase. The time between two collisions is large; therefore, the motion of the particles is considered to be statistically independent. This regime is called the dilute regime and is encountered only at low solid volume fractions $\alpha_2 < 0.001$.

  Depending on their relaxation times the particles behave differently from the gas turbulence. If τ_{12}^{F} is very large, particles are not affected by the gas turbulence. But if $\tau_{12}^{\mathrm{F}} \ll \tau_1^{\mathrm{t}}$ the particles act like fluid elements.
- $\tau_1^{\mathrm{t}} > \tau_2^{\mathrm{t}}$: the granular motion is slightly perturbed by the presence of the gas. This situation emerges at large solid volumetric fractions $\alpha_2 > 0.1$. This is the dense or collisional regime. In this case, the internal momentum transport in the solid phase is dominated by particle–particle collisions. If τ_{12}^{F} is very large then the gas–particle interactions are small. However, if $\tau_{12}^{\mathrm{F}} \simeq \tau_2^{\mathrm{t}}$, then the motions of the two-phases are coupled.
- $\tau_1^{\mathrm{t}} \simeq \tau_2^{\mathrm{t}}$: the gas–particle and particle–particle interactions are in competition. This intermediate regime is called the kinetic regime. If $\tau_{12}^{\mathrm{F}} \ll \tau_1^{\mathrm{t}}$, the motion of the particles is controlled by the turbulence of the gas. In the opposite case, $\tau_1^{\mathrm{t}} \ll \tau_{12}^{\mathrm{F}}$, the fluctuating motion of each phase is uncorrelated but the gas influences the transport properties of the particles by limiting their mean free path when $\tau_{12}^{\mathrm{F}} \ll \tau_2^{\mathrm{c}}$.

5. Application

5.1. Riser geometry—operating conditions

The simulation of an elementary situation, a two-dimensional riser, is proposed in order to evaluate the predictive capabilities of the present model. Geldart group A particles are transported with air at standard temperature and pressure. The phases are considered inert with no thermal phenomenon. The physical characteristics of each phase are summarized in Table 1.

The geometric configuration is representative of the configuration of a catalytic cracker riser (Fig. 1). The duct is two-dimensional. The solid phase is injected as dense phase at the lower part of the riser. Fluidization of the dense bed is realized by a fraction of the circulating gas. The remaining fraction, introduced above the solid inlet by two parietal injectors, propels the solid into the riser. The two-phase stream exits the riser through a right-hand elbow. The geometrical and operating conditions are summarized in Table 2.

Table 1

	Gas phase	Solid phase
ρ (kg m^{-3})	1.2	1500
ν (m^2 s^{-1})	1.8×10^{-5}	–
d (μm)	–	100
U_{mf} (m s^{-1})	–	0.005
α_{1mf} (–)		0.36
U_{tv} (m s^{-1})	–	0.33
e_c	–	0.90
Group (Geldart)	–	A

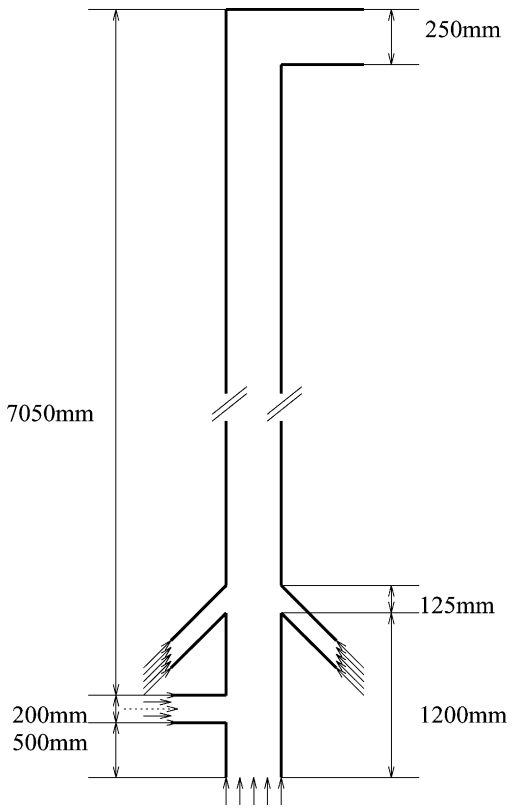

Fig. 1. Riser geometry.

Table 2

Riser height (m)	7.75
Riser width (m)	0.25
Bottom gas inlet	
Primary fluidization velocity (m s^{-1})	0.50
Parietal inlet	
Secondary fluidization velocity (m s^{-1})	10.00
Solid mass flux (kg m^{-2} s^{-1})	112.50
Outlet section	
Outlet pressure (kPa)	100.00

5.2. Boundary conditions

The model requires boundary conditions for the mean and fluctuating fields. Logarithmic velocity profiles for wall conditions are used for the gas phase. For the solid phase a slip condition is applied to the tangential component of the velocity. The fluctuating kinetic energy flux is set to zero in agreement with the assumption of elastic particle–wall collisions.

5.3. Mesh and code

The stretched Cartesian grid is composed of 45×260 nodes. The minimal size of a node, near walls, is 3 mm in both the x-direction and in the y-direction. The maximal size of a node is 12 mm in the x-direction and 25 mm in the y-direction. The time step is in the order of 10^{-2} s. The computational cost on silicon graphics solid impact is 10^{-4} s per node per sweep and per time step, that is 3 h for 20 s of flow. Calculation is performed using a commercial code, Phoenics, based on a volume difference scheme.

5.4. Results

One of the important results is the prediction of the unstable nature of the flow resulting from the development of physical instabilities causing heterogeneities in the solid volume fraction. Fig. 2 illustrates this as the cartography of the volume fraction of solids at successive time increments $\Delta t = 0.2$ s. At the base of the riser below the secondary feed a dense bed forms. Over the majority of the dense bed, the value of the solids volume fraction is approximately 15%, and less than 5% inside the bubbles. Their circulation is typical of this type of particle. The bubbles generated at the bottom of the dense bed near the walls either dissipate or rise and grow within the bed, following a non-rectilinear trajectory, before bursting at the bed surface. Their form is strongly influenced by the presence of other neighbouring bubbles and they may even coalesce.

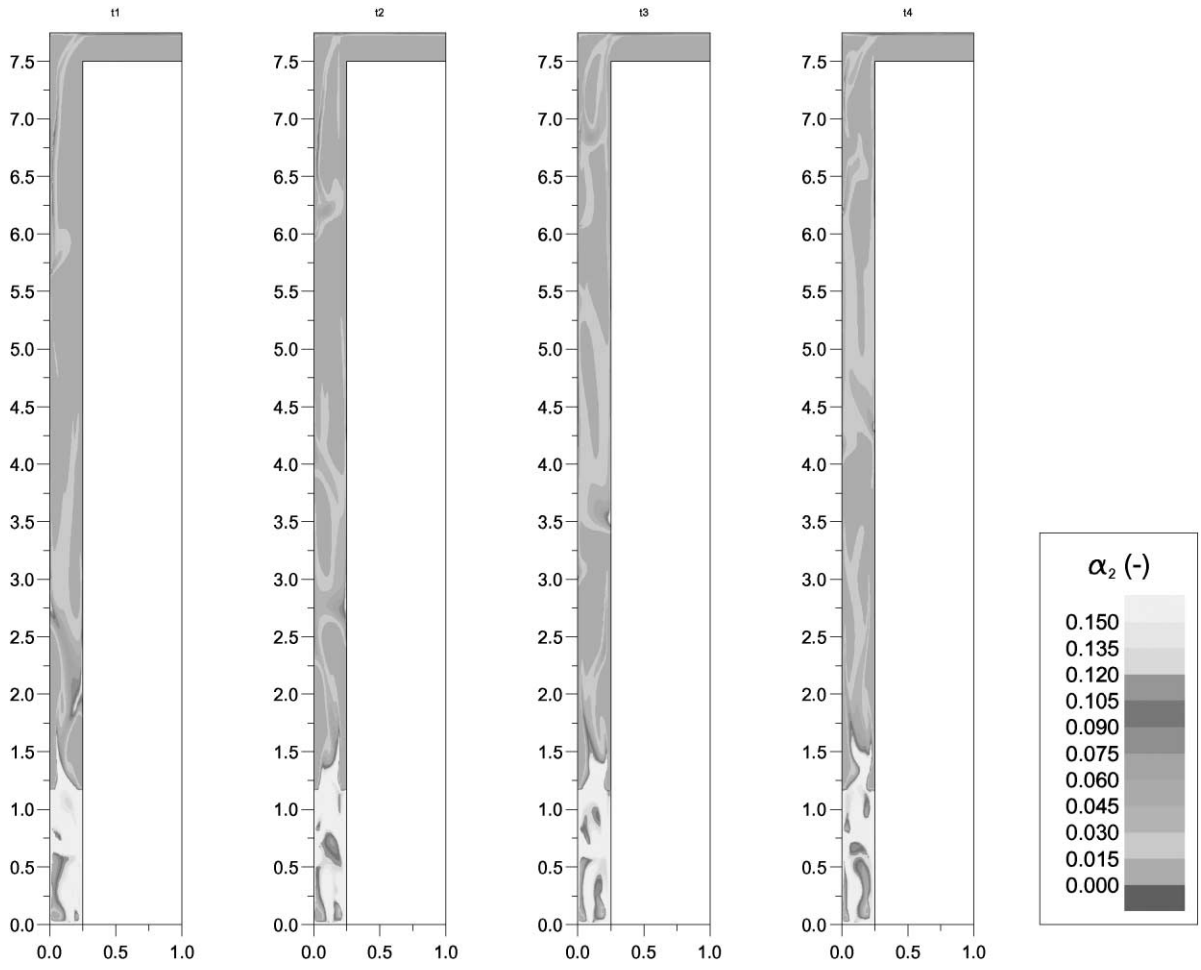

Fig. 2. Solid volumetric fraction, $\Delta t = 0.2$ s.

The secondary air injection pushes the solids from the dense bed into the riser in the form of a central jet. As it rises it breaks up, giving rise to a low concentration stream ($\alpha_2 \simeq 2\%$) at the centre and agglomerates at the wall: clusters ($\alpha_2 \simeq 10\%$). These elementary structures are in constant evolution during their transport. The physical phenomena being unstable and turbulent, a statistical analysis over a time of 10 s allows us to observe the overall behaviour of the mean values and their standard deviation:

$$X_{\text{mean}} = \frac{1}{N}\sum_{i=1}^{i=N} X_i,$$

$$\sigma_X = \frac{1}{X_{\text{mean}}}\sqrt{\frac{1}{N-1}\sum_{i=1}^{i=N}(X_i - X_{\text{mean}})^2}$$

The radial profiles are shown as a function of the geometrical parameters; widths and heights non-dimensionalized by the width of the channel.

The radial profiles of the mean solid volume fraction (Fig. 3) are representative of the core–annulus structure observed experimentally [9–12]. We observe a flat portion at the centre of the tube and a much more solid portion near the wall. The aeration of the central portion and the accumulation of particles at the wall increases along the height of the riser. The presence of an elbow at the outlet breaks the symmetry of the radial particle concentration profile which is largest at the outside of the elbow. The profiles of the standard deviation are very large (Fig. 4). The values of 50% at

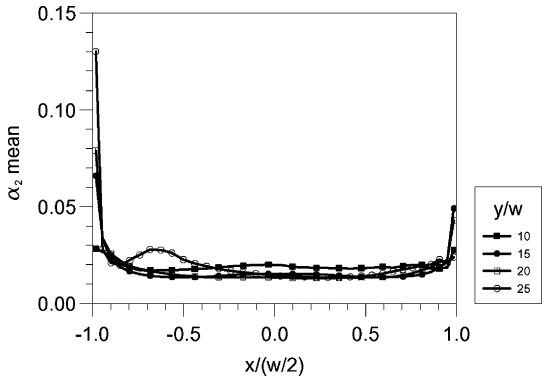

Fig. 3. Solid volumetric fraction, mean value.

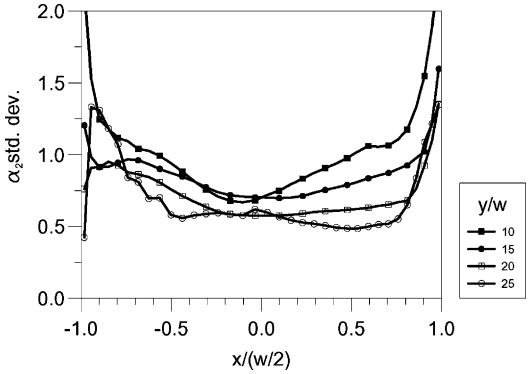

Fig. 4. Solid volumetric fraction, standard deviation.

the centre of the tube and >100% near the walls are the consequence of a fluctuating flow, and the intermittence near the wall is due to the presence of clusters. As a matter of fact, visual observations show that near the wall the solid agitation is locally damped. This implies accumulation of solids and cluster formation. Hydrodynamic characteristics of these clusters are different from isolated particles in intensity and fluctuating frequency. The temporal fluctuations of the solids fraction are very important near the secondary injector. They diminish along the height of the riser.

The mean velocity (Figs. 5–7) and the standard deviation show similar radial profiles. The form of the mean value

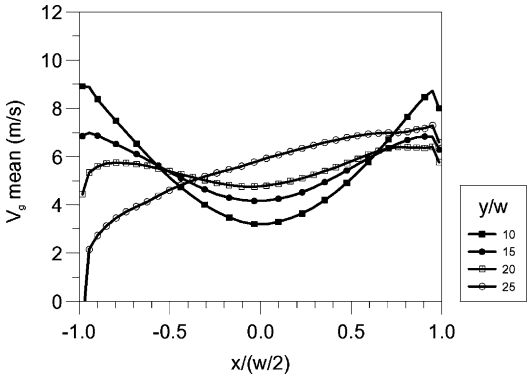

Fig. 5. Gas velocity, mean value.

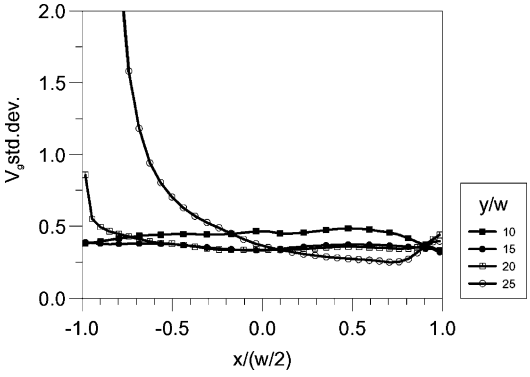

Fig. 6. Gas velocity, standard deviation.

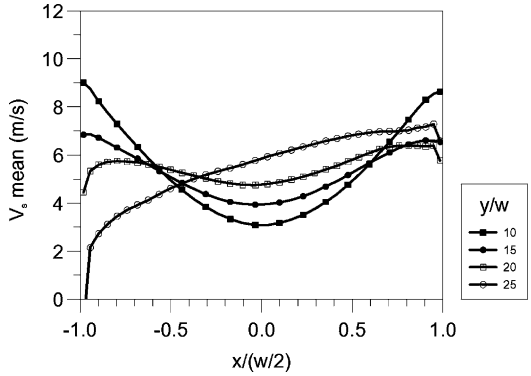

Fig. 7. Solid velocity, mean value.

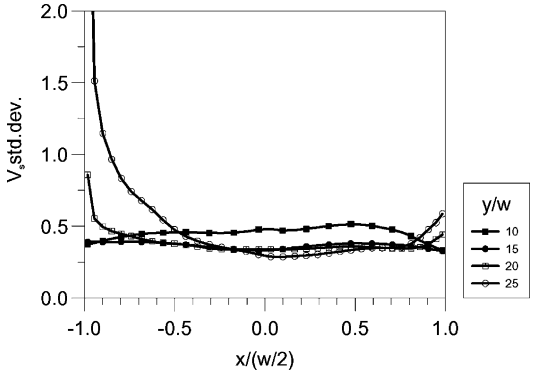

Fig. 8. Solid velocity, standard deviation.

profiles is influenced by the injectors over a large part of the riser and by the outlet conditions. At the base of the riser the profiles are symmetrical, with maximum values near the wall and minimum values at the centre. The profiles then become more uniform along the riser. Just below the outlet the profiles again become a symmetrical with the velocity varying linearly across the elbow. The mean velocity of the solids is always smaller than the gas velocity; their difference being the same order of magnitude as the terminal velocity of the particles. The spatial evolution of the profile along the riser due to the inlet and outlet conditions does not allow for a fully established flow to be obtained. The radial profiles of the standard deviation of the mean velocity are uniform, with an important value of around 30% for the region influenced by the initial conditions (Fig. 8). In the upper section, near the outlet, the profiles become a symmetrical, with an important increase in the fluctuating nature of the flow for the low-velocity zone near the outside of the elbow.

6. Conclusion

The hydrodynamic behaviour of a dilute gas–solid flow was modelled using a two-fluid model and the kinetic theory of gases to represent the transport properties of the solid phase.

Comparative study of the fluctuation time of each phase showed a collisional fluidization regime where the internal momentum transfer in the solid phase is dominated by collisions and a kinetic regime in which the fluid–particle and particle–particle interactions by collision are in competition. The asymptotic behaviour of the model is consistent with the limiting cases of a very dilute flow and a granular flow in the absence of gas.

The simulation of an elementary two-dimensional riser using Geldart group A particles illustrates the ability of the model to represent dilute gas–solid flow. The simulation results show the highly unsteady state of the flow. Inspection of the kinematic parameters fluctuations confirms these results. The core–annulus structure and the existence of agglomerates is well predicted.

The flow is never fully established and is strongly influenced by the outlet geometry in the upper portion of the riser.

References

[1] G. Balzer, O. Simonin, Extension of Eulerian gas–solid flow modelling to dense fluidized bed prediction, in: P.L. Viollet (Ed.), Proceedings of the Fifth International Symposium on Refined Flow Modelling and Turbulence Measurements, Presses de l'Ecole Nationale des Ponts et Chaussées, Paris, 1993, pp. 417–424.

[2] G. Balzer, A. Boelle, O. Simonin, Eulerian gas–solid flow modelling of dense fluidised bed, ISEF Fluidisation VIII, Tours, 1995, pp. 1125–1135.

[3] G. Balzer, O. Simonin, A. Boelle, J. Lavieville, A unifying modelling approach for the numerical prediction of dilute and dense gas–solid flow, Circulating Fluidized Bed V, Beijing, 1996.

[4] R. Clift, J.R. Grace, E. Weber, Bubbles, Drops and Particles, Academic Press, New York, 1978.

[5] S. Ergun, Fluid flow through packed bed columns, Chem. Eng. Prog. 48 (1952) 89.

[6] S. Chapman, T.G. Cowling, The Mathematical Theory of Non-uniform Gases, Cambridge University Press, Cambridge, 1970.

[7] H. Grad, On the kinetic theory of rarified gases, Commun. Pure Appl. Math. 2 (4) (1949) 331–407.

[8] J. He, O. Simonin, Non-equilibrium prediction of the particle phase stress tensor in vertical pneumatic conveying, ASME FED Gas Solid Flows 166 (1993) 253–263.

[9] A. Miller, D. Gidaspow, Dense vertical gas–solid flow in a pipe, AIChE J. 38 (11) (1992).

[10] A. Samuelsberg, B.H. Hjertager, An experimental and numerical study of flow patterns in a circulating fluidized bed reactor, Int. J. Multiphase Flow 22 (3) (1996) 575–591.

[11] J.J. Nieuwland, M. van Sint Annaland, A.M. Kuipers, P.M. van Swaaij, Hydrodynamic modeling of gas–particle flows in riser reactors, AIChE J. 42 (6) (1996) 1569–1582.

[12] A. Tinaburri, Hydrodynamic model for short contact time circulating fluidized bed, AIChE J. 42 (12) (1996) 3310–3317.